ISSN 1063-7729, Astronomy Reports, 2008, Vol. 52, No. 7, pp. 558–575. © Pleiades Publishing, Ltd., 2008.
Original Russian Text © V.V. Shimanskii, N.V. Borisov, S.A. Pozdnyakova, I.F. Bikmaev, V.V. Vlasyuk, N.A. Sakhibullin, O.I. Spiridonova, 2008, published in Astronomicheskiĭ Zhurnal, 2008, Vol. 85, No. 7, pp. 623–641.

Fundamental Parameters of BE UMa Revised

V. V. Shimanskii[1,2], N. V. Borisov[2], S. A. Pozdnyakova[1], I. F. Bikmaev[1], V. V. Vlasyuk[2], N. A. Sakhibullin[1], and O. I. Spiridonova[2]

[1] *Kazan State University, ul. Kremlevskaya 18, Kazan, 420008 Russia*

[2] *Special Astrophysical Observatory, Russian Academy of Sciences, Nizhniĭ Arkhyz, Karachaĭ-Cherkessian Republic, 357147 Russia*

Received July 23, 2007; in final form, October 26, 2007

Abstract—We have determined a complete set of parameters for the young pre-cataclysmic variable BE UMa from a comprehensive photometric and spectroscopic analysis using model atmospheres. Our precise photometry and spectroscopy were acquired with the 6-m telescope and Zeiss-1000 telescope of the Special Astrophysical Observatory and the 1.5-m Russian–Turkish telescope at a wide range of orbital phases, including times of primary eclipses. We performed a detailed identification of emission lines of ten elements. At phases of minimum brightness, the spectra reveal absorption lines and molecular bands formed in the secondary's atmosphere, whose effective temperature was determined to be $T_{eff}^{(2)} = 4750 \pm 150$ K. We have studied the radial-velocity curves of the cool star using lines of various elements. All the curves exhibit the previously predicted distortions due to reflection effects in the close binary. The derived component-mass ratio is $q = 0.43 \pm 0.09$, and the component masses are $M_1 = 0.59 \pm 0.07\ M_\odot$ and $M_2 = 0.25 \pm 0.08\ M_\odot$. We analyzed the light curves using model atmospheres for irradiated stars; all the parameters of BE UMa were refined. We demonstrate the validity of our modeling of the binary's spectra at phases of brightness maximum, which provides a good description of the observed intensities of most lines of heavy elements. The abundances of helium and several light elements (C, N, O, Ne, Mg) in the atmosphere of the cool star are probably higher than the solar values. We conclude that the physical characteristics of the primary are in good agreement with evolutionary tracks for planetary-nebula nuclei, and that the secondary is overluminous by a factor of 30 compared to main-sequence stars of the same mass.

PACS numbers: 97.80.Gm, 97.80.Hn, 97.80.Fk, 97.10.Ex, 97.10.Tk, 95.85.Kr
DOI: 10.1134/S1063772908070056

1. INTRODUCTION

According to current views, pre-cataclysmic variables (PCVs) are a fairly heterogeneous group of detached binaries after the common-envelope stage, consisting of a white-dwarf or hot-subdwarf primary and a late-spectral-type secondary [1]. This configuration gives rise to reflection effects whose amplitudes depend mainly on the hot star's luminosity [2]. For this reason, a rare group of young objects, planetary-nebula nuclei, is especially distinguished among PCVs. Reflection effects in the continuum can reach 1^m or more for young PCVs, whose spectra display numerous emission lines of hydrogen, helium, and strongly ionized heavy elements. Quantitative analyses provide a large amount of information on the physics of such systems, as well as their orbital parameters and chemical compositions, and also represent a solid base for testing and improving modern model-atmosphere techniques for describing irradiated stars and their spectra. In the future, these techniques can become a serious auxiliary tool for studies of more complex objects with reflection effects, such as polars, massive X-ray binaries, symbiotic stars, etc. Thus, the problem of accurately determining the fundamental characteristics of young PCVs, especially the "standard" object BE UMa, gains significance for our understanding of the physics operating in many kinds of close binaries.

Currently, BE UMa is the best-studied object of its class. Its variability was discovered by Kurochkin [3] who initially classified the star as a Cepheid with a period near $P = 2.29^d$. However, observations by Ferguson et al. [4] and Margon at al. [5] demonstrated the presence of a flat blue continuum and numerous narrow emission lines of HI, HeI, HeII, CII, CIII, an NIII in its spectra, as is characteristic of cataclysmic variables. At the same time, its brightness variations were strictly periodic, without any signs of quasi-periodic oscillations, flickering, or line-strength variations synchronous with brightness

variations, and its lines displayed small Doppler half-widths ($\Delta V_{Dop} < 200$ km/s), suggesting variability that was different from that usual for classical semi-detached systems.

The broadband photometry of Ando et al. [6] showed that BE UMa undergoes eclipses with durations of about $\Delta\varphi = 0.02$ and depths that increase from $\Delta m = 1.1^m$ at $\lambda\lambda$ 5265–6005 Å to $\Delta m > 4.5^m$ at $\lambda\lambda$ 3380–3700 Å. In addition, the star's light curves exhibit smooth, nearly sinusoidal brightness variations whose amplitude increases with wavelength, with no sign of secondary eclipses. As a result, Ando et al. [6] suggested that the system consists of a hot subdwarf and a cool star, with strong reflection effects.

The first quantitative estimates of the component parameters were made by Crampton et al. [7], who used emission lines of various elements to derive the cool star's radial-velocity amplitude, $K_2 = 102 \pm 3$ km/s. They noted that the main obstacle to determining the system parameters was that no features due to the radiation of the hot subdwarf were present in the spectra. Because of this, parameters were derived by analyzing the observed light curve [6] together with radial velocities using empirical mass–luminosity relations for hot subdwarfs and cool subgiants. Crampton et al. [7] estimated the temperature and radius of the primary to be $T_{eff}^{(1)} = 130\,000 \pm 13\,000$ K, $R_1/R_\odot = 0.028 \pm 0.008$ and of the secondary to be $T_{eff}^{(2)} = 3500 \pm 300$ K, $R_2/R_\odot = 2.0 \pm 0.4$.

Ultraviolet spectra of BE UMa were first studied by Hutchings and Cowley [8] using IUE observations at various orbital phases. Their spectra demonstrated no considerable variations with phase, and contained no spectral lines due to either of the components. A blackbody approximation suggested that the temperature of the hot subdwarf was significantly in excess of $T_{eff}^{(1)} = 50\,000$ K.

Studies of BE UMa have benefited since the 1990s from the use of modern CCDs and methods for numerical modeling of stellar spectra. Ferguson and James [9] undertook a detailed identification of optical emission lines, and demonstrated that the abundance ratios for CNO elements were nearly solar, so that OII lines dominated the object's spectra. Their numerical modeling using the PHOENIX code and taking into account irradiation of the stellar atmospheres gave an integrated luminosity for the hot component of $\log(L_1/L_\odot) = 2.88 \pm 0.08$, essentially coincident with more recent estimates. Based on a simultaneous analysis of brightness and line-strength variations, they determined the temperature and radius of the secondary to be $T_{eff}^{(2)} = 5050 \pm 550$ K and $R_2/R_\odot = 0.96 \pm 0.22$. These are currently the most relable estimates of the cool star's characteristics, confirming the effectiveness of the model-atmosphere technique for irradiated stars. At the same time, Ferguson and James [9] assumed that the secondary was a main-sequence star, resulting in overestimates for the masses of both components: $M_1 = 0.90 \pm 0.04\ M_\odot$ and $M_2 = 0.83 \pm 0.10\ M_\odot$.

A detailed study of the shape and amplitude of the eclipses in the system based on simultaneous $UBVR$ photometry was performed by Wood et al. [10]. They demonstrated the presence of only partial eclipses of the hot subdwarf, and derived the orbital inclination and relative radii of the components: $i = 82.4° \pm 0.1°$, $R_1/A = 0.0078 \pm 0.0001$, $R_2/A = 0.138 \pm 0.001$. Analysis of the mid-eclipse fluxes from BE UMa yielded only a rough estimate of the cool star's spectral type, G8–K4. At the same time, Wood et al. [10] found that, for the possible range of component-mass ratios, the components could not overfill their Roche lobes, and accretion in the system was impossible.

Liebert et al. [11] obtained deep CCD images of the field of BE UMa in the Hα, [OIII] $\lambda\lambda$ 5007, 4959 Å lines and discovered a rarefied shell with a radius of $r \approx 1.5$–2.0 pc. This shell, which is the remnant of a planetary nebula, confirms the evolutionary similarity of the system to other young PCVs, but suggests a relatively old age. Liebert et al. [11] observed the object spectroscopically both during and outside of eclipses. Their spectral analysis based on non-LTE model-atmosphere computations and synthetic spectra yielded the atmospheric parameters of the hot star $T_{eff}^{(1)} = 105\,000 \pm 11\,000$ K, $\log g_1 = 6.5 \pm 0.25$, and $[\mathrm{He/H}] = 0.0 \pm 0.25$.

Ferguson et al. [12] attempted to obtain a final set of fundamental parameters for BE UMa. They estimated the amplitude of the radial velocity of the primary using the Doppler shifts of the HeII λ 1640 Å absorption line. This yielded the first estimates of the component-mass ratio ($q = 0.51$) and masses of the stars, $M_1 = 0.70 \pm 0.07\ M_\odot$ and $M_2 = 0.36 \pm 0.07\ M_\odot$. In their subsequent numerical analysis of the light curves, they re-determined all the parameters of the system [12]. However, the results of this analysis must be considered doubtful: for the effective temperature derived for the cool star ($T_{eff}^{(2)} = 5800 \pm 300$ K), its absorption lines should be observable in the entire optical spectral range.

The inconsistency of the parameter set of [12] initiated additional studies of BE UMa. For example, Raguzova et al. [13] analyzed the binary's light

curves and refined some of its parameters. In particular, the temperatures of the components were found to be $T_{eff}^{(1)} = 125\,000 \pm 13\,000$ K and $T_{eff}^{(2)} = 5400 \pm 400$ K—20 and 10% different from those obtained by Ferguson et al. [12].

Thus, despite the availability of extensive studies of BE UMa, no unified set of reliable parameters exists. Moreover, different studies suggest values for each of the parameters that differ by 25%, or even 200%! This has made it difficult to construct a complete model of the system, to clarify the physics of its common-envelope phase, and to determine the time elapsed since the ejection of the envelope. Our current study attempts to resolve these problems.

Section 2 briefly describes our spectroscopic and photometric observations and reduction techniques. Section 3 is devoted to an analysis of the observed spectra, including a detailed identification of the observed emission lines and estimation of the temperature of the cool star. Section 4 presents radial-velocity measurements based on lines of various elements and the derived component masses. The light curves of BE UMa are analyzed using model atmospheres for irradiated stars and a complete set of the binary's fundamental parameters is derived in Section 5. Section 6 considers the formation of the object's spectra taking into account reflection and non-LTE effects, and includes a chemical-composition estimate for the secondary.

2. OBSERVATIONS

2.1. Spectroscopy

Our spectroscopy of BE UMa was obtained with the 6-m telescope of the Special Astrophysical Observatory (Russian Academy of Sciences) during five runs in 1999–2006, with exposure times of 300 s in each run. The wavelength and flux calibration was done using spectra from an ArNeHe lamp and the standards HZ 44 and BD 28°4211 from the survey [14] taken at the same epochs as the data for BE UMa.

Our observations of April 8 and 10, 1999 were made at the Nasmyth-1 focus with the SP-124 spectrograph [15] and a Photometrics CCD detector (1024×1024 pixels with 24×24 μm per pixel). The B2 diffraction grating (1200 rulings per millimeter) gave a dispersion of 1.3 Å per pixel in the selected range, $\lambda\lambda$ 3920–5250 Å. The observations were performed under good weather conditions, with seeing no worse than 2″. We obtained 26 individual spectrograms of BE UMa in four series. The resulting spectral resolution was $\Delta\lambda \approx 2.6$ Å, and the mean signal-to-noise ratio about $SNR = 23$–25.

Our spectroscopy of April 26, 2004 was acquired with the long-slit UAGS spectrograph [15] equipped with the same CCD detector and a diffraction grating with 1302 rulings per millimeter. The spectra were taken under satisfactory weather conditions, with seeing of 3″. We selected the range $\lambda\lambda$ 3930–5100 Å, which contains the largest number of emission lines of hydrogen and heavy elements. These spectra have a dispersion of 1.2 Å per pixel and a spectral resolution of $\Delta\lambda = 2.9$ Å. In total, we obtained nine spectrograms in two series with the same signal-to-noise ratio, $SNR = 40$.

We reduced the spectrograms taken with the SP-124 and UAGS spectrographs in the standard way using the MIDAS astronomical reduction system [16].

Our spectroscopy of March 22, 2006 was obtained using the SCORPIO focal reducer for the primary focus [17] in long-slit spectroscopic mode and an EEV 42-40 CCD detector (2048×2048 pixels, pixel size 13.5×13.5 μm) mounted at the primary focus. We obtained the spectra with the VPHG1200g grism (1200 rulings per mm), giving a spectral resolution of $\Delta\lambda = 3.3$ Å at $\lambda\lambda$ 3950–5700 Å. During these observations, which were made under satisfactory weather conditions with seeing 3.0″, we obtained 10 spectrograms in two series, with the mean signal-to-noise ratio in each $SNR = 40$. We reduced the data using specialized IDL packages for astronomical data reduction.

A log of all our spectroscopic observations of BE UMa is presented in Table 1, which contains the heliocentric Julian days HJD, orbital phases φ according to the ephemeris [13], and heliocentric radial velocities of the secondary $V_r(X)$ derived from lines of various elements (see below).

2.2. Photometry

Our photometric observations of BE UMa were obtained simultaneously in the U, B, V, and R bands on April 12, 2005, March 1, May 4, May 11, and June 3, 2006, and March 14, 2007 using a multi-band photometer on the 1-m Zeiss-1000 telescope of the Special Astrophysical Observatory. These observations were made using a 2048×2048-pixel nitrogen-cooled EEV 42-40 CCD chip and broadband filters corresponding to the Cousins photometric system. The observations on April 12, 2004, June 3, 2006, and March 14, 2007 were made under good weather conditions, with seeing of about $d = 1.5$″, and those on the other nights in the presence of intermittent clouds. The main goal of these observations was precise photometry of BE UMa at eclipse phases. The

Table 1. Log of the spectroscopic observations of BE UMa: HJD is the heliocentric Julian date, φ the orbital phase according to [13], V_r(all) the heliocentric radial velocity of the secondary, and V_r(X) the relative radial velocities of the secondary found from lines of various elements

HJD 2450000+	φ	V_r(all), km/s	V_r(HI), km/s	V_r(HeI), km/s	V_r(HeII), km/s	V_r(CNO), km/s
1277.260	0.5169	−83.1	2.4	22.3	13.4	6.1
1277.265	0.5193	−92.8	−1.3	7.1	0.9	−3.4
1277.269	0.5210	−89.9	2.5	−0.6	−2.2	−11.4
1277.272	0.5226	−83.1	4.0	5.3	4.8	9.5
1277.276	0.5242	−95.3	−6.7	−0.3	−7.9	−3.4
1277.280	0.5258	−89.9	0.7	0.8	−2.2	0.7
1277.453	0.6014	−158.0	−69.4	−54.5	−67.6	−67.6
1277.457	0.6031	−158.7	−69.2	−63.1	−68.2	−67.8
1277.461	0.6047	−159.7	−69.3	−37.8	−76.6	−67.6
1277.464	0.6063	−165.2	−82.9	−47.5	−71.3	−67.2
1277.468	0.6079	−169.6	−85.3	−53.8	−72.1	−71.7
1279.236	0.3795	10.0	97.5	101.4	99.5	103.8
1279.239	0.3811	16.1	104.9	100.8	112.4	107.9
1279.243	0.3827	14.8	99.8	76.7	107.8	112.9
1279.247	0.3843	14.5	104.9	89.7	99.6	103.9
1279.251	0.3859	5.9	95.0	100.4	99.5	91.0
1279.488	0.4896	−51.2	40.1	39.0	35.5	39.1
1279.492	0.4912	−55.2	39.9	43.3	28.3	19.9
1279.495	0.4928	−57.7	37.9	35.4	13.4	28.1
1279.499	0.4944	−51.3	37.8	9.4	35.6	43.5
1279.503	0.4961	−49.1	40.2	5.4	40.0	40.4
1279.508	0.4983	−54.3	36.0	59.6	35.5	27.1
1279.512	0.4999	−51.2	40.4	16.7	61.2	0.7
1279.515	0.5016	−63.4	25.7	1.3	13.7	44.4
1279.519	0.5032	−46.0	50.3	11.3	43.0	14.3
1279.523	0.5048	−41.6	45.5	39.7	52.8	48.3
3122.232	0.7716	−186.9	−93.8	−	−97.7	−80.3
3122.238	0.7740	−170.6	−78.4	−24.4	−80.3	−62.7
3122.242	0.7759	−157.8	−65.0	−25.1	−63.2	−54.7
3122.246	0.7776	−161.2	−65.0	−30.6	−67.5	−74.6
3122.490	0.8843	−	−	−	−58.6	−30.0
3122.495	0.8861	−131.6	−53.3	−	−51.2	−
3122.499	0.8880	−140.4	−60.7	−	−20.8	−
3122.502	0.8895	−155.1	−39.4	−	−	−24.9
3122.506	0.8913	−147.6	−80.1	−	−12.8	−
3817.243	0.1152	−10.8	−	73.6	63.0	−
3817.249	0.1176	−8.1	87.0	58.7	57.1	38.3
3817.252	0.1192	−21.5	73.0	62.4	44.2	−
3817.256	0.1208	−33.7	36.9	66.9	−	23.6
3817.259	0.1224	−18.2	51.7	97.8	85.0	52.5
3817.263	0.1239	−18.2	56.9	78.7	27.7	61.7
3817.355	0.1639	2.0	94.5	131.2	95.2	60.4
3817.373	0.1717	−3.1	85.4	106.8	86.7	66.0
3817.376	0.1733	−17.2	97.1	87.6	69.7	−
3817.380	0.1749	−14.3	55.4	−	99.5	44.5

exposure times on March 1, 2006 were 100 s in V and B and 200 s in U; the exposures on the other nights were 60 s in R and 120 s in V and B. The total duration of our photometric runs during eclipses of the binary was about 12.5 hours. As a result, we acquired 212 CCD images of the field of BE UMa (16, 30, 76, and 86 in the U, B, V, and R bands, respectively) that were found to be suitable for the subsequent analysis.

We obtained R observations at out-of-eclipse phases on April 9, 2005 with the 1.5-m Russian–Turkish telescope (RTT) at the TÜBITAK National Observatory (Turkey) using the TFOSC device equipped with a nitrogen-cooled CCD chip. A technical description of the TFOSC device can be found at http://astroa.physics.metu.edu.tr/tug/tfosc.html. These observations were performed under excellent weather conditions, with seeing no worse than 1.5″. 185 images were obtained in two series (with 182 and 3 images), each with exposure times of 60 s, for a total observation duration of more than 3 hours covering the important orbital phase range $\Delta\varphi = 0.658-0.775$.

On April 30, 2007, we used the RTT to obtain quasi-simultaneous photometry of BE UMa in four bands of the standard Bessell BVR_cI_c system near maximum brightness, to verify the absence of a secondary eclipse. The detector was an ANDOR CCD chip (2048 × 2048 pixels, pixel size 13.5 × 13.5 μm) with deep thermoelectric cooling to −60°C mounted at the Cassegrain focus of the telescope. The weather conditions were good, with seeing of 1.5″. A total of 160 images were obtained in each filter, with a time resolution of 30 s and orbital-phase coverage in the range $\Delta\varphi = 0.45-0.55$.

These data were reduced using standard routines of the MAXIM-DL package. Three stars of similar brightness in the CCD field were chosen as comparison objects. An intercomparison of their brightnesses showed them to be constant within the uncertainties in the differential photometry, $\Delta m_V = 0.03^m$.

We also used the photoelectric observations by Raguzova et al. [13] performed in 1982–1994 with the 60-cm and 125-cm telescopes of the Sternberg Astronomical Observatory Crimean Laboratory to estimate the out-of-eclipse brightness of BE UMa. We rejected the data from [13] in all bands for phases $\Delta\varphi = -0.05-0.05$ and $\Delta\varphi = 0.42-0.58$ as not satisfying the claimed precision level, $\Delta m_V = 0.03^m$. However, a comparison of the eclipse-phase light curves of BE UMa from our observations and from [13] shows that they coincide within the measurement uncertainties. We will use the results of the two series of photometric data together in our subsequent analysis. The corresponding combined light curves of BE UMa in the four bands are displayed in Fig. 1.

3. ANALYSIS OF THE SPECTRA OF BE UMa

In our analysis of the spectra, light curves, and radial-velocity curves of BE UMa, we used the technique for computing the radiation of close binaries including reflection effects and externally irradiation of the model atmospheres that is realized in the SPECTR software package [18, 19], which includes computations of the surface shapes of both components based on their Roche lobes. The surfaces of each component were then subdivided into local areas with angular sizes of 5° in both directions, and the parameters of the stellar atmosphere (the effective temperature T_{eff}, gravity $\log g$, abundances of helium [He/H] and of heavy elements [M/H]) and external irradiation (its strength K_x, angle θ, and frequency distribution) determined for each. We assumed that the BE UMa primary did not experience significant irradiation, and that the frequency distribution of light incident on the secondary could be described with theoretical spectra of sdO subdwarfs with specified atmospheric parameters for $\Delta\lambda = 210-15\,000$ Å. We considered two types of chemical compositions for the atmospheres of both stars: with the solar composition and with an excess of helium and light elements. This led us to conclude that there were indeed abundance excesses for several elements in the atmosphere of the secondary (see Section 6), and so we performed our main studies of the characteristics of BE UMa allowing for its non-solar chemical composition. We computed model atmospheres for irradiated areas in the two-flux approximation for given parameters assuming a balance of the heating and cooling functions in the gas [20, 21]. The initial, non-irradiated model atmospheres were found by interpolation, using yhe technique developed in [22] and the grid of blanketed models [23]. We obtained blanketed model atmospheres of blue subdwarfs for our selected parameters using the BINARY3 code [20].

We used the model atmospheres to compute the specific intensities of the outgoing radiation at $\lambda\lambda$ 3000–9000 Å in increments of $\Delta\lambda = 0.04$ Å for three orthogonal directions, taking into account all the continuum opacity sources tabulated in the SPECTR software package [18], as well as some 580 000 lines from the list [23] and the main molecular bands found by Ya.V. Pavlenko (Main Astronomical Observatory, National Academy of Sciences of Ukraine) in accordance with the theory of Nersisyan et al. [24]. We used the Vidal–Cooper–Smith broadening theory to calculate the hydrogen line profiles [25]. Doppler broadening from thermal motions and microturbulence (assumed to be $\xi_{turb} =$

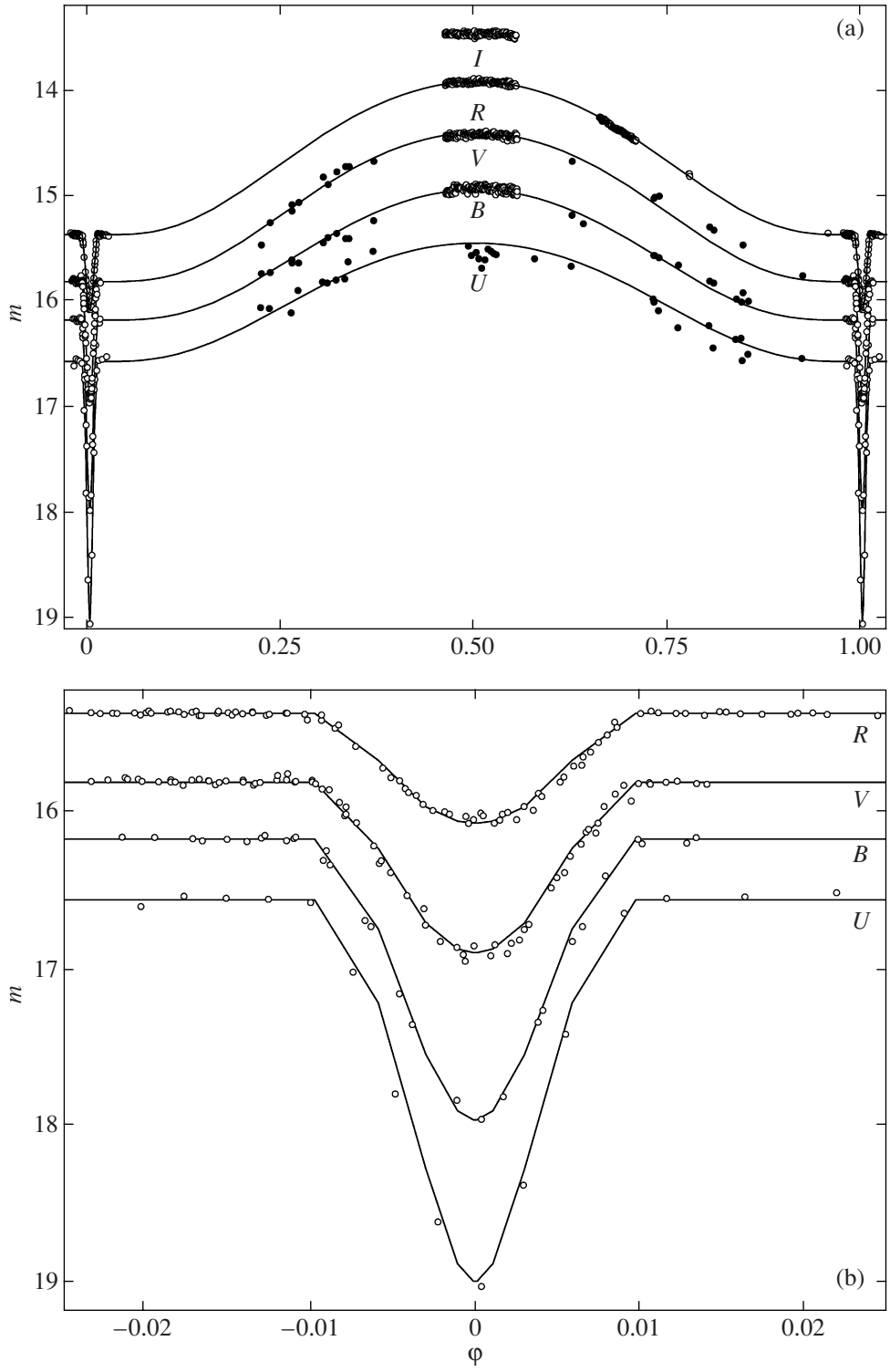

Fig. 1. Observed (circles) and theoretical (curves) light curves of BE UMa in the U, B, V, and R bands for (a) the entire orbital period and (b) the eclipse phase.

2.5 km/s), natural damping, Stark broadening specified by the approximating formula from [26], and van der Waals broadening with constants C_6 determined using the classical formula [27] with the scale factor $\Delta \log C_6 = 0.7$, were used as additional broadening factors for other lines.

We then summed the specific intensities for 72 orbital phases, interpolating them to the direction towards the observer and taking into account the sizes, velocities, and visibility conditions of the local areas. Finally, we convolved the resulting radiation fluxes with an instrumental function represented by a Gaussian whose half-width corresponded to the spectral resolution, together with the reaction curves of the Johnson system according to [28].

We normalized all the available spectrograms in the same way, using the Origin 6.1 software package. For continuum points, we chose spectral regions no narrower than $\Delta\lambda = 5$ Å that were free from emission and absorption lines with equivalent widths exceeding $W_\lambda = 30$ mÅ. These regions were chosen by comparing the spectra of BE UMa to the similar spectra of the young PCV V664 Cas from [29] and to theoretical spectra computed with the SYNTH package for the model atmospheres [23] with $T_{eff} = 100\,000$ K, $\log g = 6.5$, $[M/H] = 0.3$; $T_{eff} = 30\,000$ K, $\log g = 4.0$, $[M/H] = 0.3$; and $T_{eff} = 5000$ K, $\log g = 4.0$, $[M/H] = 0.3$. This selection of atmospheres was determined by the requirement that conditions for the formation of the radiationbe close to those on the surfaces of the components of BE UMa.

Figure 2 displays the object's spectra for selected orbital phases based on spectrograms averaged within individual time series. These show numerous emission lines of hydrogen, helium, and highly ionized heavy elements. A comparison of Figs. 1 and 2 shows that all the line intensities vary synchronously with the brightness variations, according to a nearly sinusoidal law. Thus, the emission spectrum of BE UMa is formed solely due to reflection effects near the hot spot on the surface of the secondary. The object's absorption spectrum is observable only at minimum brightness ($\Delta\varphi = 0.85-0.15$), as the wings of the HI lines (Hβ, Hγ) and HeII ($\lambda\lambda$ 4686, 5411 Å), as well as numerous weak lines and blends of neutral atoms of heavy elements and molecular bands at $\lambda >$ 4900 Å. As we will demonstrate below, these molecular bands are formed on the non-irradiated part of the secondary's surface, and can be used to directly determine its atmospheric parameters.

To compile as complete a list of emission lines in the spectrum of BE UMa as possible, we averaged 17 spectrograms at phases with the strongest reflection effects, $\Delta\varphi = 0.48-0.52$. The resulting spectrum has $SNR \approx 140$, and is compared in Fig. 3 with the spectra of the young PCVs V664 Cas and Abell 65. We identified the lines in this spectrum by comparing it to the spectra of V664 Cas [29] and V1357 Cyg [30] and to a grid of theoretical spectra computed using the SYNTH code for a series of model atmospheres [23] with $T_{eff} = 25\,000-33\,000$ K and various chemical compositions. The complete list of identified lines with their equivalent widths is presented in Table 2. We can see that there is no doubt that the binary's radiation contains emission lines of eight elements (H, He, C, N, O, Ne, Mg, Si), and probably two more elements as well (Al, S). Note that, compared to the similar systems VW Pyx [31] and TW Crv [32], the HI, HeII lines and all singlet HeI lines in BE UMa are stronger by factors of 1.4–2.5. We also detected enhanced intensities for lines of O, Ne, and Si, which provide indirect evidence for excess abundances of these elements in the atmosphere of the secondary. These excesses could be related to the object's initial chemical composition, as well as the dredge-up of matter, synthesized in the primary, during the common-envelope phase [33].

The line-intensity ratios for elements in different ionization stages can be used to estimate the mean gas temperature in the line-formation region, which proves to be $T_e = 17\,000-22\,000$ K, or $\Delta T_e \approx 3000$ K lower than in V664 Cas [29]. In general, we confirm the conclusion of Ferguson and James [9] that the BE UMa spectra are dominated by lines of singly rather than doubly ionized CNO atoms. Thus, the extremely strong reflection effect in this system is due to an increased size and better visibility of the hot spot, rather than to strong surface heating of the secondary.

Our observations at minimum brightness, $\varphi = 0.12$, were extended to $\lambda = 5700$ Å. A preliminary analysis of the spectra revealed numerous heavy-element absorption lines in the longwave part, due to the cool star (Fig. 4). We modeled the spectrum at $\lambda\lambda$ 4800–5500 Å by varying the effective temperature of the cool component, $T_{eff}^{(2)}$, to obtain the best agreement between the observed and theoretical line intensities. The main parameters for BE UMa were adopted according to [9, 10]. We varied the ratio of the component radii simultaneously with $T_{eff}^{(2)}$ in order to keep the contribution from the cool component constant. The best agreement between the observed and theoretical spectra, shown in Fig. 4, was achieved for $T_{eff}^{(2)} = 4750 \pm 150$ K. Note that, not only were the strengths of all significant absorption features at $\lambda > 5150$ Å satisfactorily modeled in this case, but the proportions of the intensities of lines of heavy elements (such as MgII $\lambda\lambda$ 5172, 5183 Å) and molecular bands (λ 5207 Å), which are sensitive to temperature variations, were preserved. Our $T_{eff}^{(2)}$ value lower than those derived by Ferguson and James [9] ($T_{eff}^{(2)} = 5000 \pm 500$ K), Wood et al. [10] (spectral type K1), or Raguzova et al. [13] ($T_{eff}^{(2)} = 5400 \pm 450$ K),

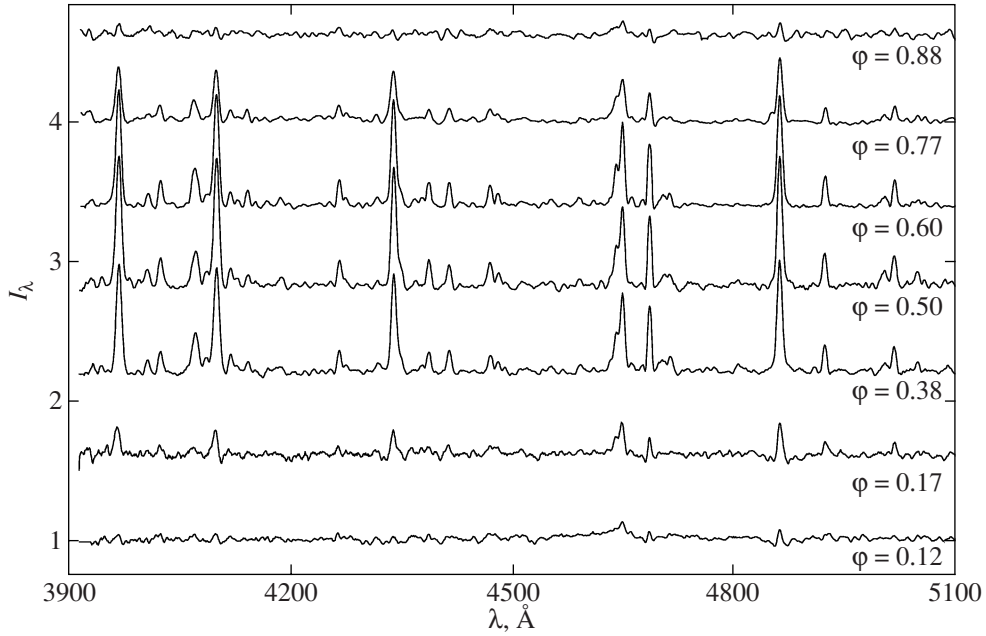

Fig. 2. Normalized observed spectra of BE UMa for orbital phases $\varphi = 0.12, 0.17, 0.38, 0.50, 0.60, 0.77$, and 0.88. Subsequent spectra are shifted by 0.6 along the vertical axis.

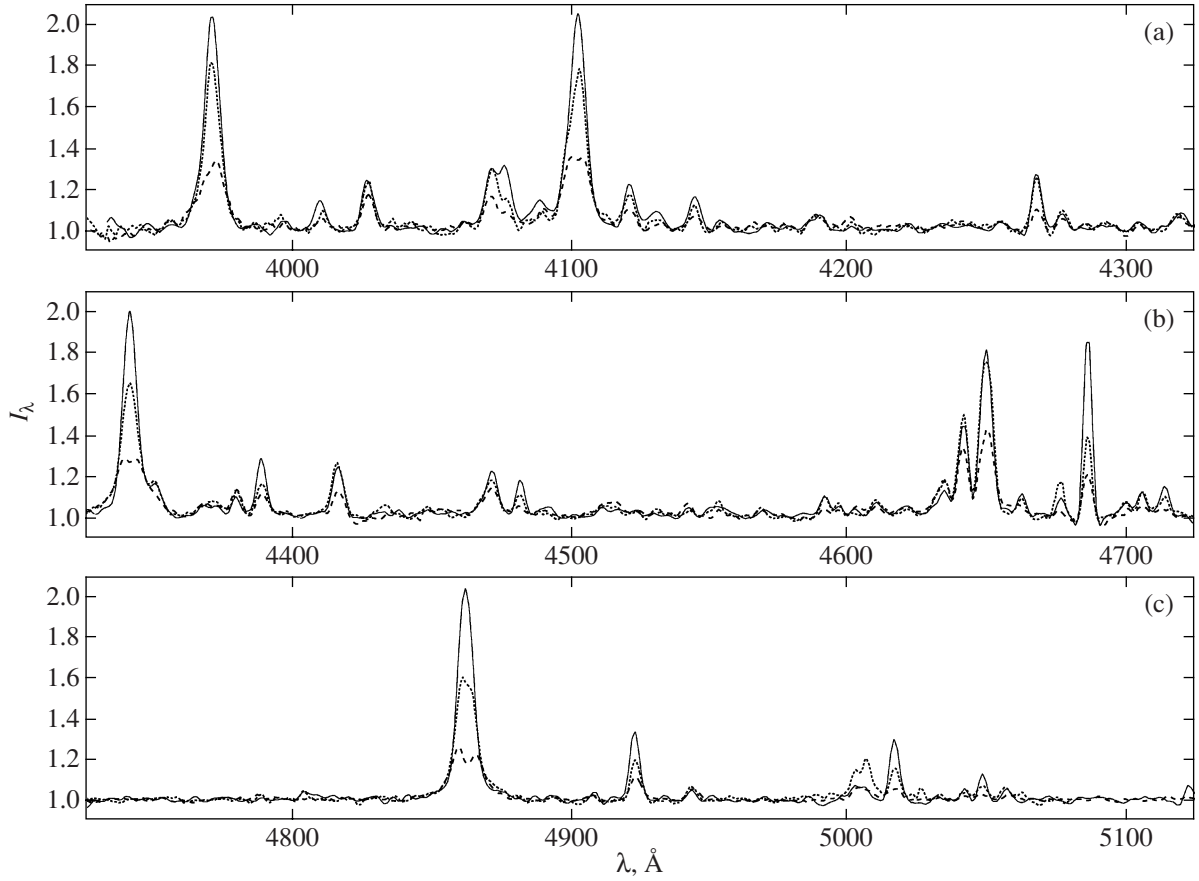

Fig. 3. Averaged observed spectrum of BE UMa (solid line) at maximum brightness, $\Delta\varphi = 0.48-0.52$, compared to the spectra of young PCVs V664 Cas (dashed line) and Abell 65 (dotted line).

Table 2. Lines identified in the spectrum of BE UMa: $\Delta\lambda$ and W_λ are the wavelength and equivalent width in the averaged spectrum for phases $\Delta\varphi = 0.48{-}0.52$

λ, Å	W_λ, Å	Identification	λ, Å	W_λ, Å	Identification
3937.46	0.015	NIII (3839)	4371.92	0.199	CII (4372)
3946.61	0.093	OII (3945)	4378.82	0.403	OII (4378)
3955.65	0.116	OII (3954), NII (3955)	4387.88	1.275	HeI (4387)
3970.05	7.788	HI (3970)	4395.10	0.125	OII (4395)
3984.62	0.132	OII (3982), SIII (3983)	4405.37	0.022	SiIII (4405)
3995.89	0.171	NII (3995)	4409.07	0.096	CII (4410), NeII (4409)
4008.74	0.701	HeI (4009)	4415.49	1.208	OII (4414, 4416)
4026.03	1.295	HeI (4026)	4428.17	0.028	NeII (4428, 4430)
4033.79	0.079	NII (4035)	4431.46	0.099	NII (4432)
4044.30	0.062	NII (4041, 4043)	4437.36	0.099	HeI (4437)
4060.51	0.163	OII (4060, 4061)	4447.68	0.212	NII (4447), OII (4446, 4448)
4069.66	1.121	OII (4069, 4072)	4457.29	0.096	NeII (4457)
4087.65	0.720	OII (4089), SiIV (4088)	4461.97	0.114	OIII (4461)
4101.76	7.860	HI (4101)	4470.76	1.336	HeI (4471), OII (4465, 4467)
4120.40	1.124	HeI (4120), OII (4119, 4121)	4481.24	0.715	MgII (4481), Al (4479)
4129.54	0.630	OII (4132)	4487.97	0.141	OII (4488, 4489)
4143.77	0.803	HeI (4143), OII (4141, 4145)	4500.88	0.028	OII (4500)
4153.35	0.187	OII (4153), CIII (4152)	4510.55	0.171	NIII (4510)
4170.34	0.145	HeI (4168), OII (4169)	4516.46	0.223	CIII (4515, 4516)
4177.58	0.053	SiIII (4178)	4522.55	0.101	NeII (4522), NIII (4523)
4185.31	0.174	OII (4185)	4528.86	0.068	NII (4530), AlIII (4528, 4529)
4189.29	0.270	OII (4189)	4533.62	0.016	NIII (4434, 4435)
4200.40	0.034	HeII (4199)	4541.83	0.159	HeII (4541)
4206.06	0.020	NeII (4206)	4552.15	0.446	SiIII (4552)
4220.80	0.103	NeII (4219)	4569.32	0.155	SiIII (4567)
4233.39	0.164	NeII (4233)	4575.32	0.018	SiIII (4574)
4241.90	0.134	NII (4241)	4590.93	0.436	OII (4591)
4254.19	0.158	OII (4253, 4254)	4596.18	0.169	OII (4596)
4267.11	1.168	CII (4267)	4601.72	0.140	OII (4602), NII (4601)
4276.11	0.334	OII (4275, 4276, 4277)	4609.70	0.347	OII (4609), NII (4607)
4283.14	0.020	OII (4283)	4620.14	0.364	CII (4618, 4619)
4290.29	0.095	OII (4291)	4633.81	0.860	NII (4630), SiIV (4631)
4294.81	0.056	OII (4294)	4640.91	1.927	OII (4638, 4641), NIII (4640)
4303.86	0.155	OII (4302, 4303)	4649.05	4.342	CIII (4647, 4650), OII (4649)
4312.73	0.036	OII (4313)	4661.81	0.435	OII (4661)
4318.90	0.489	OII (4317, 4319)	4669.02	0.077	OII (4669)
4340.49	6.967	HI (4340)	4676.02	0.321	OII (4676)
4349.35	1.084	OII (4347, 4349, 4351)	4685.65	3.221	HeII (4685)
4367.11	0.279	OII (4366, 4369)	4699.33	0.350	OII (4699)
4705.25	0.484	OII (4705)	4892.36	0.105	OII (4890)
4713.30	0.659	HeI (4713)	4907.44	0.114	OII (4906)
4733.83	0.029	CII (4734, 4735)	4914.83	0.054	NeII (4913)
4746.96	0.038	CII (4747)	4922.05	1.485	HeI (4921)
4752.04	0.041	OII (4751)	4942.56	0.173	OII (4941, 4943)
4787.97	0.032	NII (4788)	4949.93	0.076	SiIV (4950)
4803.19	0.174	NII (4803)	5002.79	0.570	NII (5001, 5005)
4813.94	0.097	SiIII (4813)	5015.72	1.270	HeI (5015)
4819.47	0.049	SiIII (4819)	5030.84	0.062	NeII (5032)
4828.46	0.078	SiIII (4828)	5040.93	0.163	NeII (5039)
4861.07	6.702	HI (4861)	5047.48	0.437	HeI (5047), NII (5045)

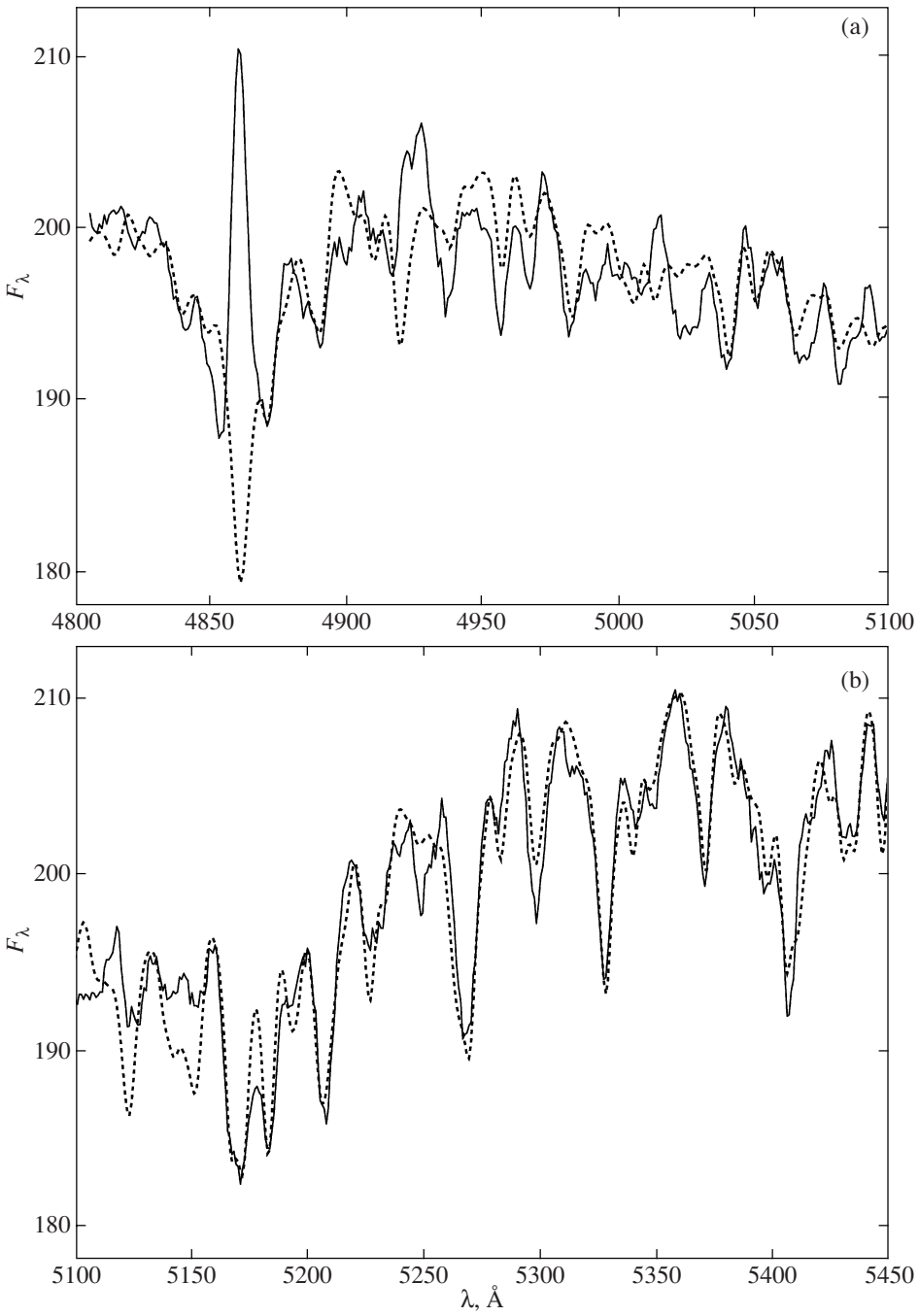

Fig. 4. Average observed (solid curve) and theoretical (dashed curve) spectra of BE UMa at minimum brightness ($\varphi = 0.12$) at $\lambda\lambda$ 4800–5450 Å.

agrees with the estimate of Liebert [11] (spectral type K5), and is considerably higher than the estimate of Crampton et al. [7] ($T_{eff}^{(2)} = 3500$ K). However, these studies derived the temperature from the observed light curves of BE UMa, which yield uncertainties not better than $\Delta T_{eff}^{(2)} = \pm 400$ K [13]. For this reason, we use our derived $T_{eff}^{(2)}$ in all of our subsequent analysis.

4. ANALYSIS OF RADIAL VELOCITIES OF BE UMa

We applied the cross-correlation technique to measure the radial velocity of the secondary, $V_r^{(2)}$. Figure 2 show that only the emission cores of the Hβ, Hγ and HeII λ 4686 Å lines and the emission blend at $\lambda\lambda$ 4630–4660 Å are observable simultaneously at minimum and maximum brightness. Therefore, we

restricted our cross-correlation analysis to intervals $\Delta\lambda = 30$ Å widths containing these lines, centered on their laboratory wavelengths. We used the average spectrum at maximum brightness, $\Delta\varphi = 0.48{-}0.52$, presented in Fig. 3 as a comparison spectrum. We measured the radial velocities for the lines listed above both together and separately for lines of different elements: HI (Hβ, Hγ), HeII (λ 4686 Å), CNO ($\lambda\lambda$ 4630–4660 Å), HeI ($\lambda\lambda$ 4367, 4471, 4921, 5017 Å). The results are presented in Table 1 and Fig. 5.

Our analysis of the derived $V_r^{(2)}$ values shows that their variations with orbital phase do not agree with a circular orbit for the binary. The corresponding fit shown in Fig. 5a differs considerably from the observed radial velocity curve, whose extrema are closer to phase $\varphi = 0.50$. As a result, the gradient of $V_r^{(2)}$ exceeds the analogous gradient at phase $\varphi = 0.00$ by a factor of two, as is characteristic of systems with elliptical orbits. Our fit for the elliptical-orbit model, with the eccentricity $e = 0.14 \pm 0.01$ and periastron passage close to phase $\varphi = 0.50$, is in good agreement with all the observations (Fig. 5a). However, a significantly eccentric orbit seems improbable for a binary after the common-envelope stage. At the same time, Abubekerov et al. [34] showed that the radial-velocity curves of binaries with strong reflection effects and non-spherical components should be strongly distorted, with their extrema displaced towards $\varphi = 0.00$ or $\varphi = 0.50$, depending on the type of line considered. Similar distortions of their V_r curves were detected earlier for two young PCVs with strong reflection effects, V664 Cas [29] and TW Crv [32]. Thus, we believe that the orbit of BE UMa is actually nearly circular. Our estimates of the center-of-mass radial velocity and the secondary's radial-velocity amplitude in the circular-orbit model ($\gamma = -74.5 \pm 2.9$ km/s, $K_2 = 101.2 \pm 4.7$ km/s) are in good agreement with those of [7] ($\gamma = -71 \pm 2$ km/s, $K_2 = 102 \pm 4$ km/s). However, this amplitude corresponds to the motion of an area inside the hot spot on the surface of the secondary, rather than to motion of the secondary's center of mass. A more accurate estimate of the $V_r^{(2)}$ amplitude ($K_2 = 105.7 \pm 3.0$ km/s) results from the fit for the elliptical-orbit model. We computed a series of spectra for BE UMa at various phases, taking into account the reflection effect, for the set of binary parameters of Ferguson and James [9] in order to accurately estimate differences in the radial velocities of the secondary and the hot spot on its surface. These computations were carried out using the SPECTR software package described above. Our analysis of line shifts in the theoretical spectra shows that, when the secondary's rotation is synchronous with its orbital motion, the K_2 value derived for a circular orbit requires a correction of $\Delta K_2 = 5.1$ km/s. The final radial-velocity amplitude for the secondary is $K_2 = 106.3 \pm 4.7$ km/s, in full agreement with the value derived for the elliptical orbit.

Figures 5b, 5d show that the radial velocities measured from the HI and HeII lines agree very well. The smaller K_2 amplitude derived from the HeII lines is due to the formation of these lines in the central part of the hot spot. The CNO emission blend ($\lambda\lambda$ 4630–4660 Å) shows a lower amplitude, $K_2 = 95.6 \pm 3.9$ km/s. This is due to the absence of the blend in the absorption spectrum of the primary, which leads to artificial shifts of the HI and HeII emission lines. Note that the center-of-mass velocities, orbital eccentricities, and times of periastron passage coincide for the three $V_r^{(2)}$ sets, within the uncertainties. We detected an unexpected difference only for the HeI lines, which display a radial-velocity curve with a lower amplitude, $K_2 = 86.2 \pm 4.7$ km/s, a center-of-mass velocity higher by $\Delta\gamma = 23$ km/s, and a significantly different shape of the elliptical orbit. Since we found these differences both for all the studied HeI lines together and for each separately, they cannot be due to wavelength-calibration uncertainties, noise, or errors in the cross-correlation analysis. At the same time, in the adopted physical model for BE UMa, the HI and HeI lines should form under similar conditions and display equal radial velocities. Thus, the reason for the V_r differences for the lines of these elements remains unclear.

We estimated the component-mass ratio by comparing the binary's average spectra at minimum brightness, $\varphi = 0.12$ and $\varphi = 0.88$ (Fig. 2), when weak absorption wings of the Hβ, Hγ, and HeII λ 4686 Å lines were observed. Preliminary calculations of the spectra of BE UMa show that the HI absorption profiles can be associated with both components. Thus, only the HeII λ 4686 Å line can be used for radial-velocity estimates. We performed our cross-correlation analysis of this line manually, separately fitting its emission and absorption components at various phases. For the absorption component, we used the parts of the profile within $\Delta\lambda = 6{-}12$ Å of the line center. This yields differences for the heliocentric velocities of the two emission components $\Delta V_r^{(2)} = 82 \pm 6$ km/s and of the two absorption components $\Delta V_r^{(1)} = 35 \pm 8$ km/s. Thus, the component-mass ratio is $q = \dfrac{M_2}{M_1} = \dfrac{\Delta V_r^{(1)}}{\Delta V_r^{(2)}} = 0.43 \pm 0.09$. This value agrees with the estimate of [12] ($q = 0.50 \pm 0.06$) within the uncertainties.

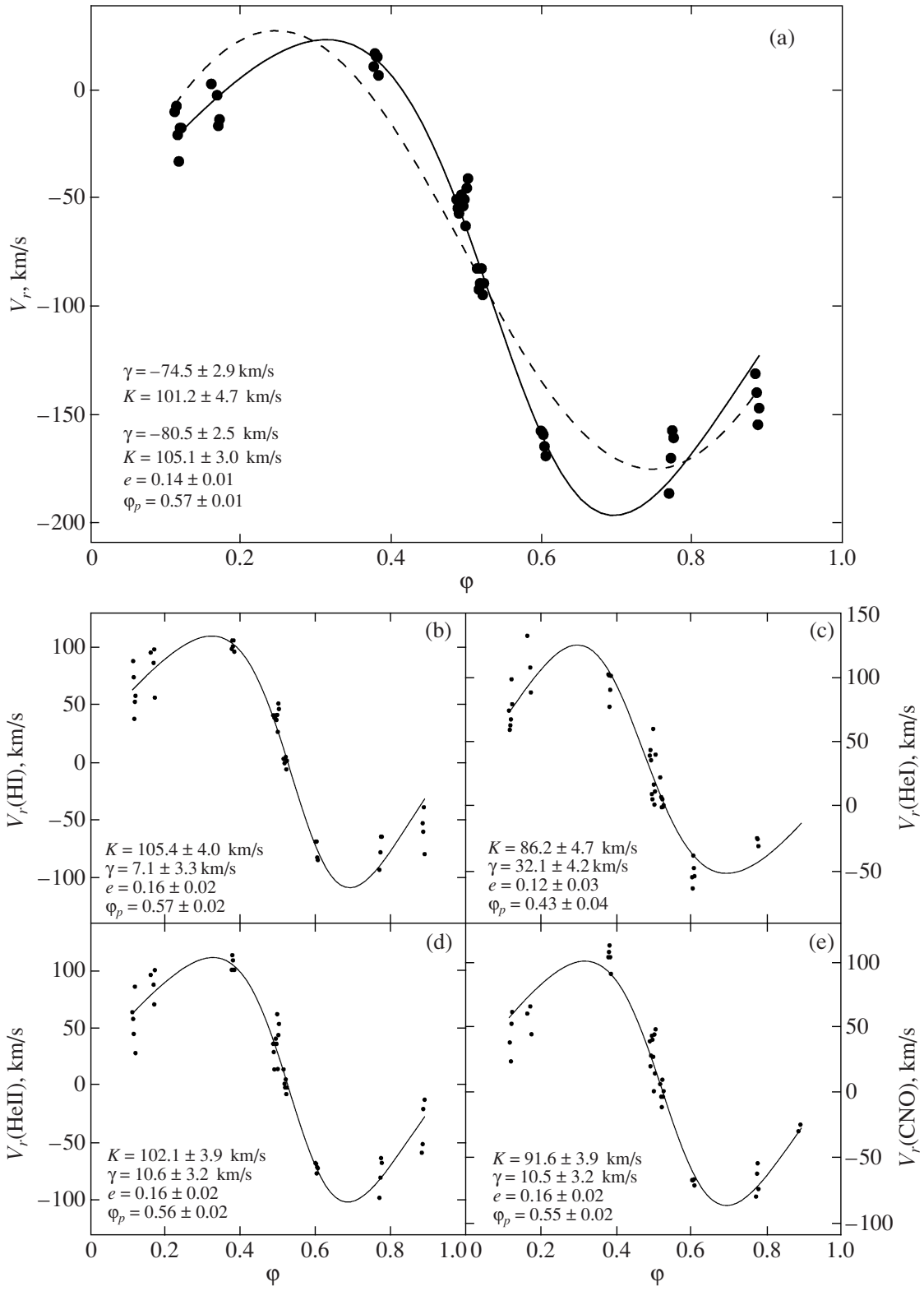

Fig. 5. Radial-velocity curves of BE UMa from lines of different elements: (a) simultaneously from HI, HeII lines and the CNO blend; (b) from the Hβ and Hγ lines; (c) from the HeI $\lambda\lambda$ 4367, 4471, 4921, 5017 Å lines; (d) from the HeII λ 4686 Å line; (e) from the $\lambda\lambda$ 4630–4660 Å CNO blend. The points show the observations, while the dashed and solid curves are approximations assuming circular or elliptical orbits, respectively. The approximation parameters are indicated in each panel. Panels (b)–(e) present relative velocities.

Table 3. Parameters of BE UMa ("*" marks data from [13], and "1" and "2" parameters derived for the circular- and elliptical-orbit models)

Parameter	Component	
	Primary	Secondary
P_{orb}, days	$2.2911667^* \pm 0.0000007$	
φ_0, JD	$2447628.5381^* \pm 0.0003$	
K, km/s	–	$106.3^1 \pm 4.7$
		$105.1^2 \pm 3.0$
γ, km/s	–	$-74.5^1 \pm 2.9$
		$-80.5^2 \pm 2.5$
e	0.14 ± 0.01	
ω	$203° \pm 3°$	
q	0.43 ± 0.09	
T_{eff}, K	$123\,000 \pm 5000$	4750 ± 150
$\log g$	6.90 ± 0.02	3.90 ± 0.10
$M/M_\odot$	0.59 ± 0.07	0.25 ± 0.08
$R/R_\odot$	0.046 ± 0.002	0.94 ± 0.03
$A/R_\odot$	6.89 ± 0.14	
i	$82.6° \pm 0.2°$	

The derived radial-velocity amplitude, combined with the improved orbital period, $P_{orb} = 2.2911667^{\rm d}$ [13], determine the mass function of the primary, $f(M_1) = 0.281 \pm 0.023\ M_\odot$. Using the measured mass ratio and the orbital inclination from the light-curve analysis of Wood et al. [10], $i = 82.4° \pm 0.1°$, we found the dynamical masses of the BE UMa components to be $M_1 = 0.59 \pm 0.07\ M_\odot$ and $M_2 = 0.25 \pm 0.08\ M_\odot$. The semimajor axis derived from these masses, $A = 6.89 \pm 0.14 R_\odot$, agrees with the results of Ferguson et al. [12] within the errors ($A = 7.5 \pm 0.5 R_\odot$). The main uncertainty in the derived mass estimates still comes from uncertainty in the radial velocities measured for the primary. Improving the precision of estimates of M_1, M_2, and A will require a long series of observations of the HeII λ 4686 Å line profiles at minimum brightness that can be subject to a cross-correlation analysis.

5. ANALYSIS OF THE LIGHT CURVES OF BE UMa

The amount and precision of our photometric data are sufficient to determine all the unknown parameters of the components based on an analysis of the light curves of BE UMa (Fig. 1). In particular, our Zeiss-1000 CCD observations at $\Delta\varphi = -0.022 \ldots -0.014$ enable correct estimation of the eclipse amplitude, duration, and phase in the four studied bands. The photoelectric data of [13] show an out-of-eclipse asymmetry of the light curve that is different in the U, B, V bands, which was, however, not confirmed by other authors [6]. Thus, we used these observations only to estimate the amplitudes of the reflection effect, and determined the out-of-eclipse shape of the light curve solely from our RTT-150 observations in the R band.

In general, fitting the observed and theoretical eclipse amplitudes enabled us to derive the temperature of the primary, $T_{eff}^{(1)}$, the eclipsed part of the primary, s, and the component-radius ratio, $\dfrac{R_2}{R_1}$ for a given temperature of the secondary $T_{eff}^{(2)}$. However, for primary temperatures higher than $T_{eff}^{(1)} = 60\,000$ K, its $U-B$, $B-V$, and $V-R$ color indices become independent of $T_{eff}^{(1)}$, so that $T_{eff}^{(1)}$ cannot be derived from the eclipse amplitude. At the same time, the availability of four observed amplitudes for two desired parameters (see above) made it possible to check the correctness of the adopted value of $T_{eff}^{(2)}$. The resulting fit between the observed and theoretical eclipse profiles, displayed in Fig. 1b, is achieved for $\dfrac{R_2}{R_1} = 20.6 \pm 0.7$ and $s = 0.892 \pm 0.053$. Thus, the eclipse of BE UMa is not total, in agreement with the conclusion of Wood et al. [10], and our temperature estimate for the secondary is sufficiently accurate.

Modeling the eclipse shape and duration together with the earlier derived parameters yielded the orbital inclination, $i = 82.6° \pm 0.2°$, and the ratio of the two component radii to the semimajor axis, $R_1/A = 0.0067 \pm 0.0003$ and $R_2/A = 0.137 \pm 0.004$. Thus, the component radii are $R_1/R_\odot = 0.046 \pm 0.002$ and $R_1/R_\odot = 0.94 \pm 0.03$. Note that the main uncertainty in these parameters is due to uncertainty in the observed eclipse shape rather than the value of $T_{eff}^{(2)}$.

Modeling of the out-of-eclipse light curves of BE UMa yielded direct estimates of the reflection effects in the system and their dependence on the component radii, semimajor orbital axis, and, most strongly, the temperature of the primary $T_{eff}^{(1)}$. Fitting the theoretical and observed brightnesses in the U, B, V, R bands and using the known parameters, we found $T_{eff}^{(1)} = 123\,000 \pm 5000$ K.

We can see from Fig. 1 that we are able to correctly reproduce the observed shape of the R light

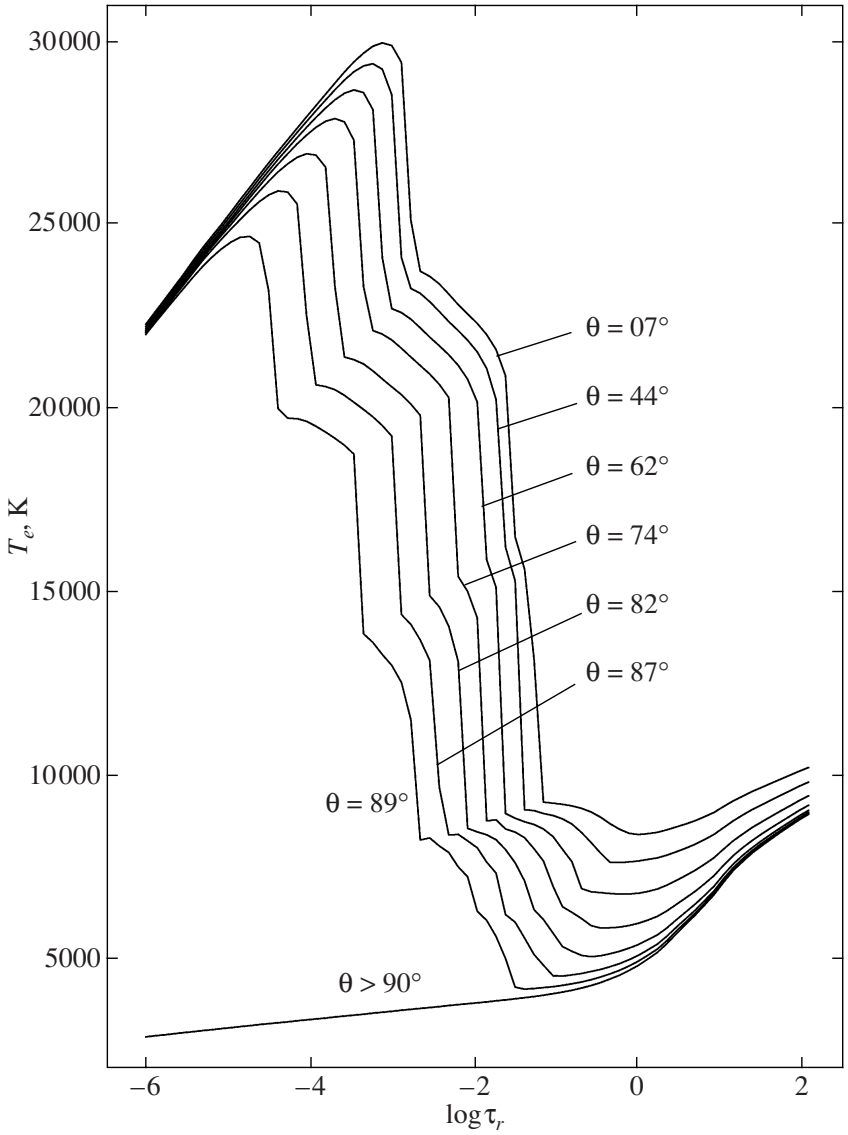

Fig. 6. Distributions of the electron temperature, T_e, in terms of the Rosseland optical depth, τ_r, in the atmosphere of the BE UMa secondary for various points inside and outside the hot spot. The angle of incidence of the external radiation is indicated.

curve, confirming the correctness of the adopted parameter set summarized in Table 3. Comparison to the results of earlier studies shows agreement for individual parameters but not for the set as a whole. The light-curve analysis of Wood et al. [10] gave similar estimates for the relative radii ($R_1/A = 0.0078 \pm 0.0001$, $R_2/A = 0.138 \pm 0.001$) and the orbital inclination ($i = 82.4° \pm 0.1°$). Ferguson and James [9] estimated the radius of the secondary to be $R_2/R_\odot = 0.96 \pm 0.22$ and the luminosity of the primary to be $\log(L_1/L_\odot) = 2.95 \pm 0.12$. Our temperature estimate for the primary agrees with that of Crampton et al. [7] ($T_{eff}^{(1)} = 130\,000 \pm 13\,000$ K), Wood et al. [10] ($T_{eff}^{(1)} = 110\,000 \pm 15\,000$ K), and Raguzova et al. [13] ($T_{eff}^{(1)} = 125\,000 \pm 13\,000$ K) but is higher than was suggested by Liebert et al. [11] and Ferguson et al. [12] ($T_{eff}^{(1)} = 105\,000 \pm 13\,000$ K). This difference can be explained by the low surface gravity for the primary adopted in the spectral analysis of [11], $\log g_1 = 6.5$. Our analysis of the uncertainties in the BE UMa parameters shows that the surface gravity must exceed $\log g_1 = 6.85$, which requires a higher temperature for correct modeling of the observed HI and HeII line strengths.

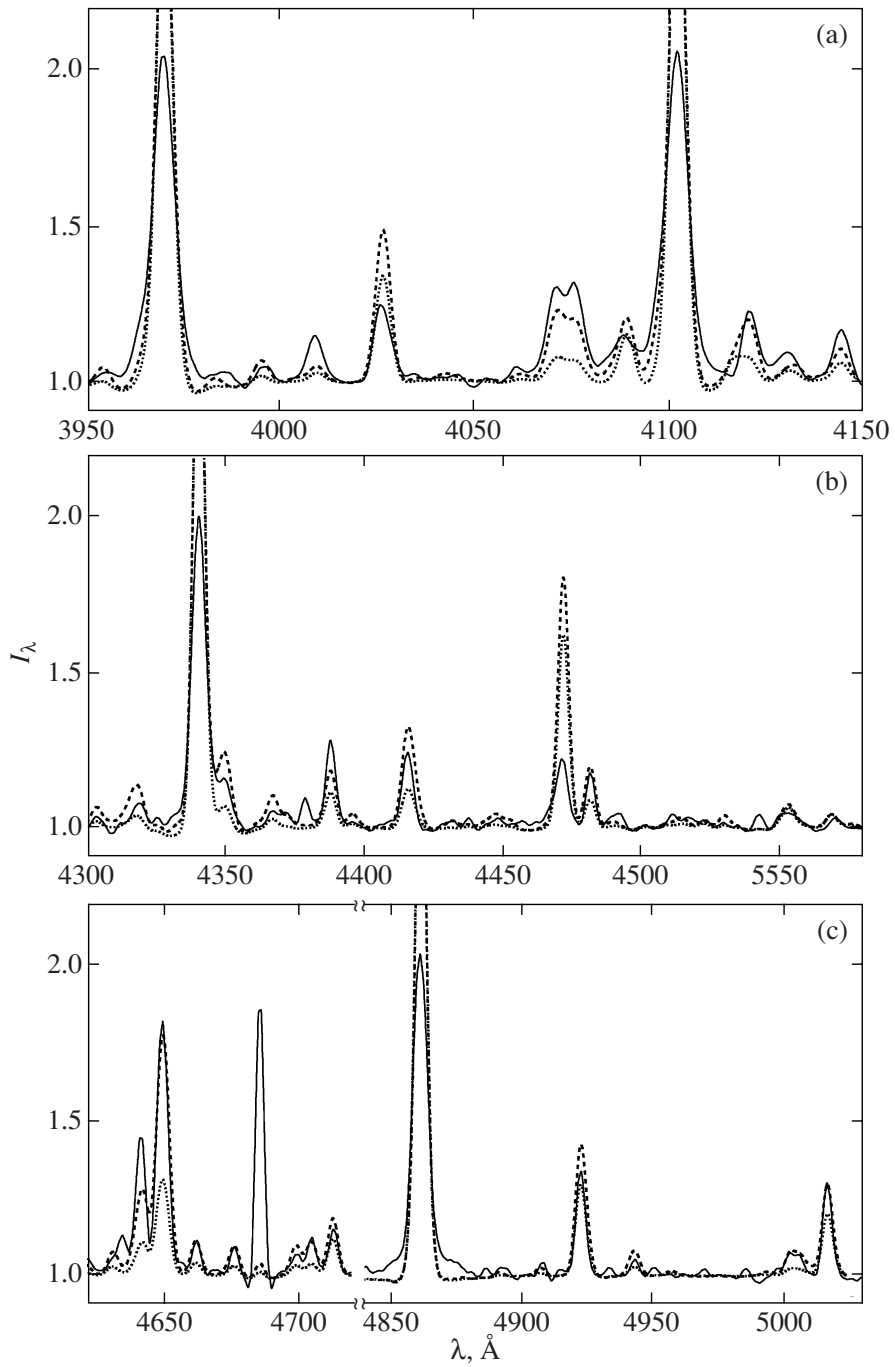

Fig. 7. Averaged observed (solid curve) and theoretical spectra of BE UMa at phases $\Delta\varphi = 0.48-0.52$. The dotted and dashed curves are the theoretical spectra for the solar and modified chemical compositions of the secondary's atmosphere (see text).

6. FORMATION OF THE BE UMa SPECTRA

Figure 6 shows the temperature distributions in the atmosphere of the secondary in various points inside and outside the hot spot. In general, these resemble the analogous distributions for other young PCVs, and show the formation of a high-temperature Lyman chromosphere at $\log\tau_r < -2.2\ldots-1.2$, as well as considerable heating of deep layers. However, the temperatures in these layers increases only to $T_e = 6500-9000$ K, while it reaches $T_e = 19\,000-21\,000$ K for the young PCVs V664 Cas [29] and V477 Lyr [35]. This slow temperature growth is due to the lower temperature of the primary in BE UMa and the larger orbital size of the system. At the same time, the

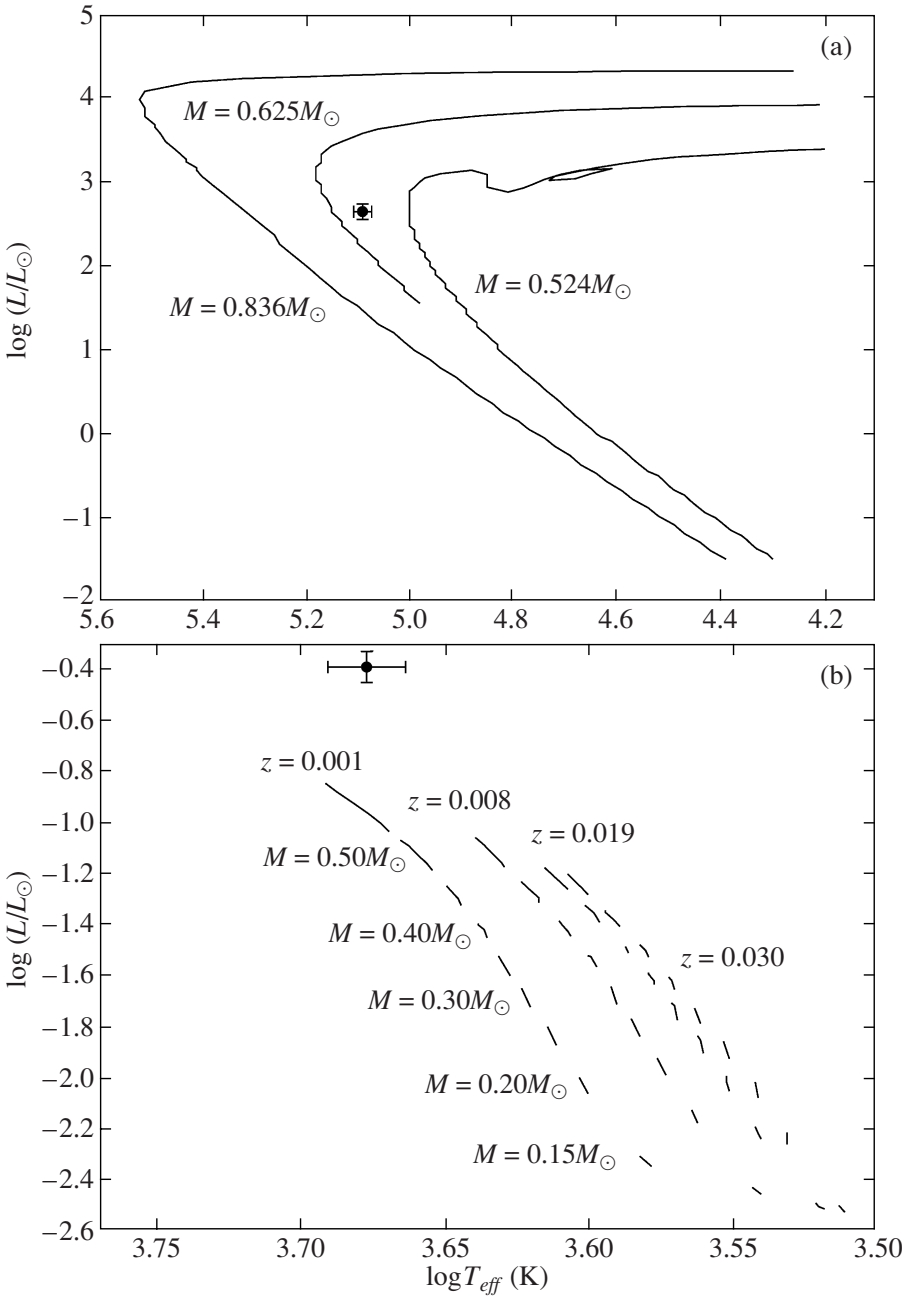

Fig. 8. Evolutionary tracks in the $\log T_{eff} - \log(L/L_\odot)$ plane for (a) planetary-nebula nuclei [38] and (b) main-sequence stars ($z = 0.030, 0.019, 0.008, 0.001$) [39]. The positions of the primary and secondary components of BE UMa are plotted as circles with error bars.

Lyman-chromosphere temperatures for all the above systems are determined by the upper temperature limit of the first temperature-instability zone [20], and are approximately the same ($T_e = 28\,000{-}31\,000$ K). Thus, an extremely non-equilibrium radiation field is formed in the atmosphere of the hot spot of BE UMa, with a considerable transfer of energy from the Lyman chromosphere to deeper layers at $\lambda\lambda$ 912–3000 Å .

The derived parameters of the binary can be used to calculate synthetic spectra assuming LTE, which are presented in Fig. 7 together with the observed spectrum for the phases of maximum brightness, $\Delta\varphi = 0.48{-}0.52$. We calculated two versions of the spectra: for a solar chemical composition for the secondary's atmosphere and assuming excesses of helium ([He/H] $= 0.2$ dex), nitrogen, and α-process el-

ements, including magnesium ([C/H], [N/H], [O/H], [Ne/H], [Mg/H] = 0.5 dex). The possible presence of such excesses is due to the enrichment of the stellar material of the secondary with the products of nuclear synthesis in the interior of the primary in the binary's common-envelope stage. A detailed analysis of the chemical composition of the old PCV V471 Tau [36] revealed excess abundances of CNO elements reaching 1.0 dex in the atmosphere of its cool star.

The spectra in Fig. 7 display a general qualitative agreement, but the following quantitative differences.

1. All the theoretical Balmer lines are enhanced by a factor of three to four in their emission cores, but possess absorption wings that are not observed.

2. Some of the HeI emission lines ($\lambda\lambda$ 4713, 4921, 5017 Å) can be described satisfactorily with the solar helium abundance, but the $\lambda\lambda$ 4026, 4471 Å triplet lines are stronger than is observed, while most singlet lines are much weaker. Increasing [He/H] increases the agreement for the $\lambda\lambda$ 4143, 4713, 5017 Å lines and other weak lines, but worsens the fit for the strongest lines ($\lambda\lambda$ 4026, 4471, 4921 Å).

3. The LTE theoretical modeling of the spectra of BE UMa does not yield even weak HeII emission lines.

4. The theoretical strengths of lines of all light elements are one-half to one-third lower than the observed strengths assuming solar abundances. This suggests that there are, indeed, excess abundances of light elements in the secondary's atmosphere. The results of our calculations for the modified chemical composition are in very good agreement with the observed spectrum for lines of both the second and third ionization stages.

Theoretical modeling of the spectra of the young PCVs V664 Cas [29] and V477 Lyr [35] gave similar results, but was able to better reproduce the observed profiles and strengths of the HI and HeII lines. One possible reason for these differences is the considerable deviations from the non-LTE that occur in the non-uniform-temperature atmosphere of the hot spot on the surface of the secondary. As was demonstrated by Ivanova et al. [37] and Barman et al. [2], the non-equilibrium radiation field in the conditions of the BE UMa secondary atmosphere leads to enhanced ionization of elements in deep atmospheric levels by a factor of 10^2–10^3 ("super-ionization"), with excess recombination of these elements ("super-recombination") in the Lyman chromosphere. As a result, when non-LTE effects are taken into account, all strong emission lines of easily ionized ions (HI and HeI) become weaker, while those of less easily ionized ions (NIII and HeII) become stronger. Note also that a relatively large amplitude for non-LTE effects in the spectra of BE UMa is favored by the low surface gravity of the secondary ($\log g = 3.8$). Thus, correct modeling of all the emission lines in the spectra of this system is possible only in an non-LTE approach.

7. CONCLUSIONS

Let us consider the derived characteristics of the BE UMa components from the point of view of modern stellar-evolution theory. Figure 8a, 8b presents the evolutionary tracks of planetary-nebula nuclei according to [38] and of low-mass main-sequence stars with various metallicities in a temperature–luminosity diagram [39]. In both cases, we also plotted the positions of the binary's primary and secondary with their error bars. Obviously, the temperature and luminosity of the sdO subdwarf correspond to a mass of $M_1 = 0.60 \pm 0.01\ M_\odot$, close to our dynamical estimate, $M_1 = 0.59 \pm 0.07\ M_\odot$. In this case, according to the models [38, 40], the lifetime of BE UMa after the ejection of its common envelope should be $t \approx 1.2 \times 10^5$ years. In general, this is in agreement with observations of the system's extended and extremely rarefied envelope, with a radius of $r \approx 1.5$–2.5 pc [11].

We can see from Fig. 8b that the secondary has a luminosity excess of about $\Delta \log L_2 = 1.5 \pm 0.2$ relative to main-sequence stars with masses $M = 0.25\ M_\odot$. This excess cannot be due to the uncertainties in the stellar parameters or chemical abundances. Moreover, a low-mass star could not complete its evolution along the main sequence and become a subgiant within the lifetime of the system. Thus, the excess luminosity of the secondary must be due to residual excitation that originated during the binary's common-envelope stage. Similar effects were found earlier for other young PCVs, such as V664 Cas [29], V477 Lyr [19], UU Sge [41], KV Vel [42], etc. Note that the cool component of BE UMa displays an excess radius, $\Delta \log R_2 = 0.53$, and, to a lesser extent, an excess effective temperature, $\Delta \log T_{eff}^{(2)} = 0.11$, while the opposite is true for the other listed systems. This is probably due to the larger orbital radius of BE UMa, which gave rise to substantial expansion of the secondary during the common-envelope stage.

ACKNOWLEDGMENTS

The authors are grateful to the Large-Telescope Allocation Committee of the Russian Academy of Sciences for their many years of support of our spectroscopic studies of close binaries. We thanks V.L. Afanas'ev for his invaluable assistance during the reduction of our observations. This study was financially supported by the Russian Foundation

for Basic Research (project no. 05-02-17744) and the State Program of Support to Leading Scientific Schools of the Russian Federation (project no. NSh-784.2006.2).

REFERENCES

1. H. Ritter, Astron. Astrophys. **169**, 139 (1986).
2. T. S. Barman, P. H. Hauschildt, and F. Allard, Astrophys. J. **614**, 338 (2004).
3. N. E. Kurochkin, Perem. Zvezdy **15**, 7 (1964).
4. D. H. Ferguson, J. Liebert, R. F. Green, and J. T. McGraw, Astrophys. J. **251**, 205 (1981).
5. B. Margon, R. A. Downes, and J. I. Katz, Nature **203**, 200 (1981).
6. H. Ando, A. Okazaki, and S. Nishimura, Publ. Astron. Soc. Jpn. **34**, 141 (1982).
7. D. Crampton, A. P. Cowley, and J. B. Hutchings, Astrophys. J. **272**, 202 (1983).
8. J. B. Hutchings and A. P. Cowley, Publ. Astron. Soc. Pac. **97**, 328 (1985).
9. D. H. Ferguson and T. A. James, Astrophys. J., Suppl. Ser. **94**, 723 (1994).
10. J. H. Wood, E. L. Robinson, and E. H. Zhang, Mon. Not. Roy. Astron. Soc. **227**, 87 (1995).
11. J. Liebert, R. W. Tweedy, R. Napiwotzki, and M. S. Fulbright, Astrophys. J. **441**, 424 (1995).
12. D. H. Ferguson, J. Liebert, S. Haas, et al., Astrophys. J. **518**, 866 (1999).
13. N. V. Raguzova, S. Yu. Shugarov, and N. A. Ketsaris, Astron. Zh. **80**, 535 (2003) [Astron. Rep. **47**, 492 (2003)].
14. R. C. Bohlin, Astron. J. **111**, 1743 (1996).
15. V. L. Afanas'ev, A. N. Burenkov, V. V. Vlasyuk, and S. V. Drabek, Preprint No. 234, SAO (Spec. Astrophys. Obs., Russ. Acad. Sci., Nizhniĭ Arkhyz, 1995).
16. P. Ballester, in *ESO/ST-ECF Data Analysis Workshop* (1992), p. 177.
17. V. L. Afanas'ev, E. B. Gazhur, S. R. Zhelenkov, A. V. Moiseev, Bull. Spec. Astrophys. Obs. **58**, 90 (2004).
18. N. A. Sakhibullin and V. V. Shimanskii, Astron. Zh. **74**, 432 (1997) [Astron. Rep. **41**, 378 (1997)].
19. V. V. Shimanskii, N. V. Borisov, and N. N. Shimanskii, Astron. Zh. **80**, 712 (2003) [Astron. Rep. **47**, 763 (2003)].
20. N. A. Sakhibullin and V. V. Shimanskii, Astron. Zh. **73**, 793 (1996) [Astron. Rep. **40**, 723 (1996)].
21. D. V. Ivanova, N. A. Sakhibullin, and V. V. Shimanskii, Astron. Zh. **79**, 433 (2002) [Astron. Rep. **46**, 390 (2002)].
22. V. F. Suleimanov, Pis'ma Astron. Zh. **22**, 107 (1996) [Astron. Lett. **22**, 92 (1996)].
23. R. L. Kurucz, *SAO CD-Roms* (Cambridge, MA, USA, 1994).
24. S. E. Nersisyan, A. V. Shavrina, and A. A. Yaremchuk, Astrofizika **30**, 247 (1989) [Astrophys. **30**, 147 (1989)].
25. C. R. Vidal, J. Cooper, E. W. Smith, Astron. Astrophys., Suppl. Ser. **25**, 37 (1973).
26. R. L. Kurucz and I. Furenlid, Spec. Rep. Smithsonian Astrophys. Obs. **387**, 1 (1979).
27. A. Unsold, *Physik der Sternatmospheren* (Springer, Berlin, 1955).
28. V. Straizys, *Multicolor Stellar Photometry* (Mokslas, Vil'nyus, 1977; Pachart Publ. House, Tucson, 1992).
29. V. V. Shimanskii, N. V. Borisov, N. A. Sakhibullin, and A. E. Surkov, Astron. Zh. **81**, 620 (2004) [Astron. Rep. **48**, 563 (2004)].
30. E. A. Karitskaya, V. M. Lyuty, N. G. Bochkarev, et al., Int. Bull. Var. Stars, No. 5678, 1 (2006).
31. K. M. Exter, D. L. Pollacco, and S. A. Bell, Mon. Not. R. Astron. Soc. **348**, 1349 (2003).
32. K. M. Exter, D. L. Pollacco, D. L. Maxted, et al., Mon. Not. R. Astron. Soc. **315**, 359 (2005).
33. V. V. Shimanskii, Astron. Zh. **79**, 145 (2002) [Astron. Rep. **46**, 127 (2002)].
34. M. K. Abubekerov, E. A. Antokhina, A. M. Cherepashchuk, and V. V. Shimanskii, Astron. Zh. **83**, 609 (2006) [Astron. Rep. **50**, 544 (2006)].
35. V. V. Shimanskii, S. A. Pozdnyakova, N. V. Borisov, et al., Letters in Astron. Zh. **36** (4) (2008).
36. N. N. Shimanskii, I. F. Bikmaev, V. V. Shimanskii, et al., in *Astrophysics and Stellar Spectroscopy* (Moscow, 2007), p. 350.
37. D. V. Ivanova, N. A. Sakhibullin, and V. V. Shimanskii, Astron. Zh. **81**, 523 (2004) [Astron. Rep. **48**, 476 (2004)].
38. J. Bloecker, Astron. Astrophys. **299**, 755 (1995).
39. L. Girardi, A. Bressan, G. Bertelli, et al., Astron. Astrophys., Suppl. Ser. **141**, 371 (2000).
40. I. J. Iben and A. Tutukov, Astrophys. J. **418**, 343 (1993).
41. D. L. Pollacco and S. A. Bell, Mon. Not. R. Astron. Soc. **262**, 377 (1993).
42. R. W. Hilditch, T. J. Harries, and G. Hill, Mon. Not. R. Astron. Soc. **279**, 1380 (1996).

Translated by N. Samus'